



AIAA 2002-1498

**Stiffness Design of Spring Back
Reflectors**

Lin Tze Tan and Sergio Pellegrino

*Department of Engineering, University of Cambridge,
Cambridge CB2 1PZ, UK*

**43rd AIAA/ASME/ASCE/AHS/ASC
Structures, Structural Dynamics, and
Materials Conference
22-25 April 2002
Denver, CO**

Stiffness Design of Spring Back Reflectors

Lin Tze Tan* and Sergio Pellegrino†

Department of Engineering, University of Cambridge, Cambridge CB2 1PZ, UK

The recently developed Spring Back Reflector has low stiffness in the deployed configuration. A general method of stiffening this type of reflector without changing its folding properties is presented. The stiffening is achieved by adding a conical skirt around the edge of the dish; this skirt snaps elastically when the dish is folded. The paper concludes that it is possible to design spring back reflectors that are up to 80 times stiffer and with a deployed fundamental frequency up to 8 times higher than in the original design.

Introduction

The newly developed Spring Back Reflector,^[1,2] shown schematically in Figure 1, consists of a thin-walled graphite mesh dish with an integral lattice of ribs and connecting elements. These components, together with a further stiffening edge beam along the rim, are made from triaxial plies of carbon-fibre reinforced plastic (CFRP). The whole structure is made as a single piece, without any expensive and potentially unreliable joints, and typically has a diameter of 6 m, thickness varying between 0.3 mm and 3.2 mm, and a total mass of around 20 kg.

The folding concept is both simple and effective: since there are no joints or hinges, opposite edges of the reflector are pulled towards each other by about half of their original distance, and thus the reflector becomes folded elastically as shown in Figure 1. It can then be stowed in the normally unused space in the nose cone of a rocket launcher. Once in orbit, the tie cables that hold the reflector in its packaged configuration are released, and the reflector deploys dynamically by releasing its stored elastic strain energy.

In order to be folded as described, Spring Back Reflectors need to have low stiffness but it is precisely their low stiffness that makes it difficult for them to achieve and retain a high shape accuracy. Furthermore, shape distortions that occur during the manufacturing of thin CFRP structures —of the order $D/1000$ in the present case— make it even more difficult to meet the stringent shape accuracy requirements imposed on communications antennas. This is a significant problem, and potentially a severe limitation on the applicability of this type of reflector. The surface accuracy of the reflector could be adjusted with mechanical devices, but this would defy the simplicity of the concept and reduce the reliability of the system.

This paper proposes a modification of the original concept, based on the idea of adding a thin-walled stiffening element around the edge of the dish. This el-

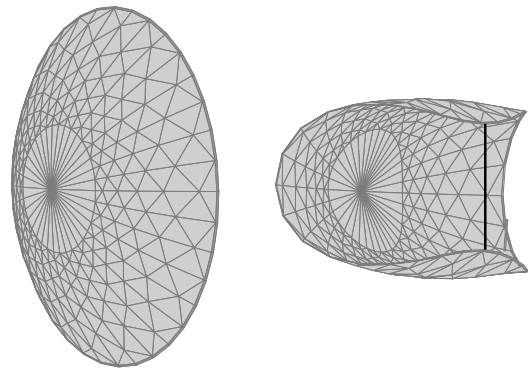


Fig. 1 Schematic views of spring-back reflector, folded and deployed.

ement significantly increases the overall stiffness of the dish in the deployed configuration, and yet its configuration is such that the stiffened dish can still be folded elastically. The viability of this approach was first demonstrated by means of simple physical models.

This paper presents a detailed finite element study of the effects of changing the various parameters of the stiffening element from which optimal configurations of a $1/10^{\text{th}}$ scale model —i.e. about 0.5 m diameter— reflector are chosen. Two selected configurations have then been physically realized and their measured properties are compared with finite element predictions.

Stiffening Method

In general, the stiffer one makes a linear-elastic structure, the “harder” it becomes to fold it elastically. This intuitive statement can be formalized using an argument based on the total strain energy in the structure being equal to the work done by two equal and opposite forces that are applied to the structure in order to fold it. If the “stiffness” is increased, the strain energy required to fold the structure by a given amount will increase proportionally. The maximum stress in the structure will also increase.

A spring-back reflector could be stiffened by increasing the stiffness of the edge rim or the ribs. However, increasing the thickness of these elements has the effect of rapidly increasing the maximum stress level in the folded reflector, whereas increasing their width is

*Research Student.

†Professor of Structural Engineering, Associate Fellow AIAA. pellegrino@eng.cam.ac.uk

Copyright © 2002 by S. Pellegrino. Published by the American Institute of Aeronautics and Astronautics, Inc. with permission.

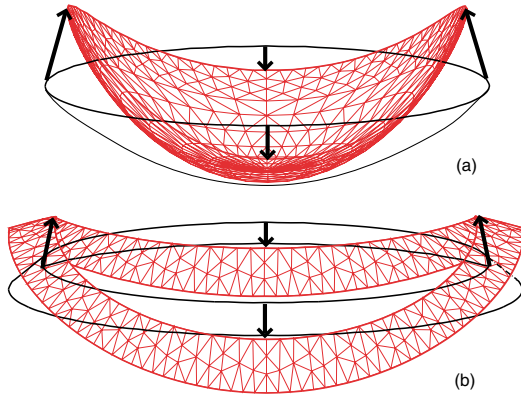


Fig. 2 Lowest stiffness, incompatible eigenmodes of dish and skirt.

inefficient in terms of mass.

An alternative, more efficient way of increasing the stiffness of a structure is to prevent it from deforming in its lowest stiffness eigenmode. In the case of an “open cap” shell this eigenmode is the inextensional, or first bending mode sketched in Figure 2(a). The associated eigenfrequency can be substantially increased by connecting the original shell to a second shell whose lowest stiffness eigenmode is geometrically incompatible with that of the first shell. In Figure 2(b) a conical shape has been chosen.

In practice, this amounts to adding a conical skirt around the original reflector, but the addition of a continuous skirt would make the reflector so stiff that it would no longer be possible to fold it. Therefore, following an approach put forward by Greschik,^[3] we counteract this effect by introducing a series of cuts, either in the skirt or in the connection between the skirt and the dish. There are many different ways of implementing this idea in practice, and in the following section we describe some pilot schemes that were explored.

Preliminary Studies

Consider a dish that has been stiffened with a small conical skirt in which some cuts have been introduced. Consider the force-displacement relationship—see Figure 7 for some examples—when two diametrically opposite points on the edge of the structure are forced to move closer together. This relationship is typically linear over a small displacement range; it then becomes non-linear and, after reaching a local maximum, the force remains approximately constant for a considerable range of displacements; for even larger displacements the force starts to increase.

There are two important parameters to be considered, as follows.

- The initial stiffness of the structure, related to its deployed stiffness, which can be characterised by computing its fundamental natural frequency. More precisely, we are interested in the ratio be-

tween the fundamental frequency, f , and the original frequency, f_0 , of the unstiffened dish.

- The highest stress in the folded configuration, σ_{max} .

A series of finite element analyses were carried out to determine how these two parameters are affected by different types and sizes of cuts. Further details on the finite element modelling of the structure will be given later, in the section Automatic Generation of Stiffening System.

First we considered the effects of introducing either two or four radial cuts in the skirt while varying the skirt width. We found that increasing the number of cuts has the effect of decreasing both σ_{max} and the ratio f/f_0 .

Next we analysed the effects of varying the angle of the conical shell, i.e. the angle between the skirt and the vertical, on σ_{max} and f/f_0 . We found that σ_{max} decreases when the skirt angle is increased from 30 deg to 110 deg. We also found that a stiffened structure with four cuts has $f/f_0 \approx 1$ for all angles in this range, whereas a structure with two cuts has $f/f_0 > 2$. Hence, we concluded that only configurations with two cuts are worth considering.

Thirdly we considered the effect of circumferential slits along the connection between the skirt and the original shell, instead of radial cuts. A particular feature of these slits is that they allow the skirt to snap through while the reflector is being folded, consequently decreasing the force required to fold the reflector and thus also significantly reducing the maximum stress level. This is due to the fact that the slits allow a large area of the dish to bend, whereas the radial cuts tend to localise the deformation around the apex of the cuts. Furthermore, these slits cause only a minor reduction in the natural frequency in the deployed configuration, compared to that of a reflector with a skirt which is continuously attached to the rim of the reflector.

Optimization

Thus far we have presented a problem, proposed a particular type of solution which includes some adjustable design parameters, and observed some general trends on how different parameters such as the number of cuts, the skirt angle and width might affect the final solution. However, in order to obtain a proper engineering solution, we need to carry out a more formal search of the design space. Figure 3 defines the five parameters to be optimised, which are

- the angles α, β defining the length of the two sets of slits;
- the angle γ defining the inclination of the skirt;
- the width w of the skirt; and

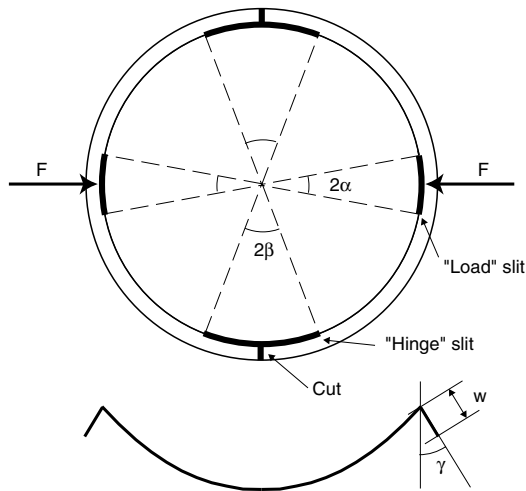


Fig. 3 Design parameters.

- the length of the cuts (which can be either 0 or w).

All of these parameters, apart from the length of the cuts, can be varied over a wide range; more details are given later in this section.

Due to the number of parameters to be optimized and the complexity of each step in the optimization process, considering a simultaneous variation of all parameters is not feasible. Hence, two types of designs, which had shown the most promise during the preliminary study, were selected and for each design optimal configurations were sought. These two designs are as follows.

- Configuration A. Two cuts and four slits of equal length ($\alpha = \beta$).
- Configuration B. Four slits of general lengths ($\alpha \neq \beta$), but no cuts.

Optimization Routine

Because there is no known analytical relationship between the design parameters, the easiest approach is the direct search method. The particular optimization method that was chosen was the Hooke and Jeeves (HJ) method,^[4] which has the advantage of not requiring the evaluation of gradients of the objective function and hence is particularly suited for problems where solutions can only be obtained numerically.

Figure 4 lists the various steps and decisions involved in this search method. It is available as a routine, written in C,^[5] which incorporates improvements made by various authors.^[6-8]

Verification of Routine and ABAQUS Interface

Haftka and Gürdal^[9] consider a linear-elastic cantilever beam with uniform, rectangular cross-section of breadth b and height h , loaded by a unit shear force at the tip. Their objectives are (i) to minimize the

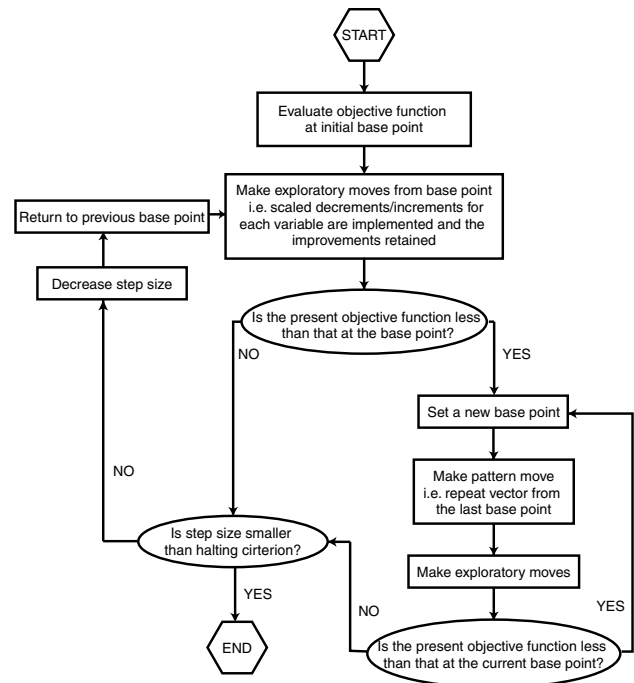


Fig. 4 Flow chart of Hooke and Jeeves method.

beam cross-sectional area, bh , while (ii) also minimizing the maximum shear stress in the beam, for which they use the expression $\tau = 3/2bh$.

Considering equal weights for these two objectives, the objective function is

$$F_{obj} = bh + \frac{3}{2bh} \quad (1)$$

and the optimum^[9] is $b^*h^* = 1.225$, which indicates that one dimension of the cross-section can be chosen arbitrarily. The corresponding value of the objective function is $F_{obj} = 2.45$.

As an initial test, to verify that the HJ optimization routine is capable of repeatable and correct convergence, the objective function in Equation (1) was programmed into the HJ routine. Several different sets of starting points were given and convergence to the values $b^*h^* = 1.225$ and $F_{obj} = 2.45$ was obtained in all cases; two examples are listed in Table 1.

Next, an interface between the optimization routine and the ABAQUS finite element package^[10] was developed and tested on the same example problem. However, this time the maximum shear stress in the beam was taken from the ABAQUS simulation, instead of using the approximate analytical expression in Equation (1).

This interface, also written in C, reads the maximum shear stress from the ABAQUS results file from the previous run, then runs the HJ routine to determine the next set of values of b and h , and then updates the ABAQUS input file accordingly; finally it makes a system call to start the next ABAQUS analysis.

The beam length was set equal to 50 units. The cross section dimensions were allowed to vary subject to the constraints

$$b > 0.5 \quad (2)$$

$$h < 5 \quad (3)$$

$$b < h \quad (4)$$

The latter condition ensures that only beam cross-sections from deep and narrow up to square are considered, thus halving the number of possible variations. These constraints were implemented via a barrier function routine which returns a very high value for the objective function if any of the variables exceeds its bounds.

The beam was modelled with 20 node quadratic brick elements (C3D20). Since the maximum shear stress occurs on the neutral axis, both the height and width of the cross section were subdivided into an odd number of elements. This is to ensure that there is always an element right at the centre of the cross-section, where the highest shear stress is reached. To prevent ill-conditioning, the number of elements was varied according to the values of b and h .

On completion of each analysis, the shear stresses in all elements were written by ABAQUS into a results file. The interface then calculates the number of the element at the centre of the beam, and another function opens the results file and searches for this particular element. The shear stress in this element is then returned to the optimization routine.

Convergence was achieved, but initially not to the expected value, see the case with Poisson's ratio $\nu = 0.3$ in Table 1. This is due to the fact that the expression for the maximum shear stress in Equation 1 is only an approximation and becomes less exact for $b \approx h$; in general, the ABAQUS approximation is more accurate. However, by setting $\nu = 0$ for the ABAQUS analysis the simple analytical expression becomes more accurate and hence a value very close to the analytical optimum was obtained, see Table 1.

Table 1 Results of optimization tests

Calculation of τ_{max}	Start points		Optimized values			
	b	h	b^*	h^*	b^*h^*	F_{obj}
Analytical	5	5	0.928	1.320	1.225	2.45
FE ($\nu = .3$)	1	1	0.993	1.223	1.225	2.45
FE ($\nu = .3$)	1	1	1.119	1.200	1.253	2.38
FE ($\nu = 0$)	1	1	1.105	1.107	1.223	2.46

Automatic Generation of Stiffening System

To carry out the optimization, an automatic method of changing the design parameters which does not require any user input was needed.

For each of the two basic designs defined previously there are four parameters to be optimized, namely α , β , γ , and w . It is worth noting that none of these

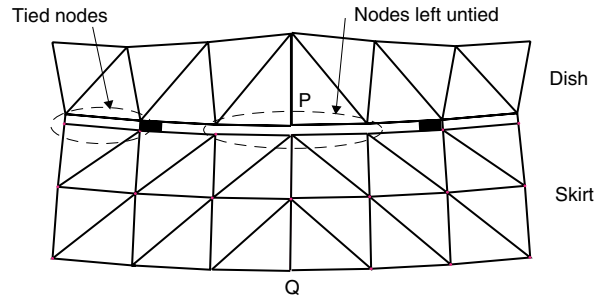


Fig. 5 Schematic of automatic mesh generation.

parameters affects the shape and design of the actual dish of the reflector; it is intended that the addition of the skirt be a relatively minor modification of the spring back reflector design. With this in mind, a quarter mesh of general 3 node shell elements (S3R) was generated for the reflector dish with PATRAN^[11] and then written to an ABAQUS input file. The nodes of this mesh were uniformly spaced on the rim, at an angle of 2 deg apart; the total number of nodes was around 600.

The skirt was then generated directly in the model input file by defining a generator starting at a point P on the rim of the dish and ending at point Q, see Figure 5. Varying the position of Q enables us to vary both the skirt angle, γ , and the skirt width, w . This generator is then rotated around the axis of the dish to define the skirt nodes in such a way that the nodes on the inner edge of the skirt are collocated with those on the rim of the dish. If cuts are to be introduced in the skirt, each separate portion is formed separately. The skirt and the dish are then connected by using the type "TIE" from the "MULTI POINT CONSTRAINT" option in ABAQUS. This option equates the global displacements and rotations of the two nodes that are tied together.

A simple way of modelling a slit would be to leave the corresponding nodes untied. However this would allow us to consider only slit lengths that are an exact multiple of the distance between rim nodes; therefore a more sophisticated technique was needed. Two additional, smaller shell elements were generated, one between each end of the slit and the first pair of dish/skirt nodes. The location of these smaller elements is calculated by a routine which, for a given set of design parameters, locates the two sets of standard dish/skirt nodes between which the end of the slit occurs. This allows the length of the slit to be varied continuously. Finally, the nodes at the end of the slit are connected to the rest of the model by using the "LINEAR" option from the ABAQUS "MULTI POINT CONSTRAINT" function. This option specifies the rotation and the displacement of a given node as a proportion of the two nodes on either side of it.

This method of automatically generating the slits was tested by considering a configuration in which the

slits terminated exactly at a dish/skirt node. Hence, for this case it was possible to use the simpler modelling technique described previously. The frequencies obtained from the two methods differed by 0.18%. The difference being due to the fact that the slit in the automatic meshing method leaves a small void in the skirt and hence the mass of this configuration is slightly lower.

ABAQUS Simulation

After setting up the ABAQUS input file two different analyses were carried out. First, the fundamental natural frequency of the structure was determined from a linear eigenvalue analysis, and second a geometrically non-linear, displacement controlled simulation of the folding process was performed, in order to find the maximum stress in the structure.

Given a structure that exhibits snapping behaviour, in general it is not obvious at which stage of folding the maximum stress, σ_{max} , will be reached. In the present case, though, an exhaustive numerical study had shown that —due to the very large deformation that is imposed after any snaps have taken place— σ_{max} for the dish occurs always in the final, fully-folded configuration of the reflector. Typically, in this configuration the two diametrically opposite points of the reflector that are pushed closer together are at a distance of $D/2$. Therefore, only the stresses in the final configuration need to be scanned by the interface routine to find σ_{max} , at the end of the folding simulation.

Note that the highest stress in the skirt given by the simulation is sometimes higher, but damage of the skirt can be avoided by carefully folding the skirt by hand, instead of pulling on the whole reflector with two concentrated forces.

Objective Function

The aim of the optimization is to maximise the fundamental natural frequency of vibration of the deployed structure, subject to a limit, σ_0 , on the maximum stress in the structure in the folded configuration. This limit was implemented through a penalty function which greatly increases the objective function if the limit is exceeded. Mathematically, this can be expressed as:

$$F_{obj} = -f + \exp(\sigma_{max} - \sigma_0) \quad (5)$$

Optimization Results

The model to be optimized is a 1 mm thick, parabolic dish with diameter $D = 450$ mm and focal length $F = 135$ mm, made from Polyethylene Terephthalate Glycol Modified, PETG (sold in sheet form, under the trade name Vivak). This material is essentially isotropic and has Young's Modulus $E = 1.86$ GPa and Poisson's ratio $\nu = 0.36$.

The following limits were placed on the design parameters of the stiffening system

- slit angles, $0.5 \leq \alpha, \beta \leq 30$ deg;
- skirt angle, $-5 \leq \gamma \leq 150$ deg;
- skirt width, $5 \leq w \leq 40$ mm.

and both Configuration A and Configuration B were investigated for different values of σ_0 .

Optimal values were found to have at least a factor of 3 increase in fundamental natural frequency, compared to the unstiffened configuration (which has $f_0 = 5.8$ Hz) for $\sigma_0 = 25$ MPa, increasing to nearly 8 for $\sigma_0 = 40$ MPa.

This optimization problem does not have a single minimum, hence to be reasonably sure that convergence to the global optimum has been achieved, for a particular value of σ_0 several optimization runs — typically 10 or more— were carried out with different starting points. At the end, the solutions with the highest frequency were selected. It was noted that the optimization usually converges to the maximum value of w , and hence in some optimization runs w was assigned a definite value, instead of being considered as a variable.

Figure 6 is a plot of the eight optimal values obtained, initially by prescribing different values for σ_0 only —points 1 to 4— and then by also prescribing $w = 20$ mm —points 5 to 8. The corresponding design parameters are listed in Table 2. Note that all eight designs have $\gamma \approx 90$ deg and there is a general trend for γ to decrease with increasing σ_0 .

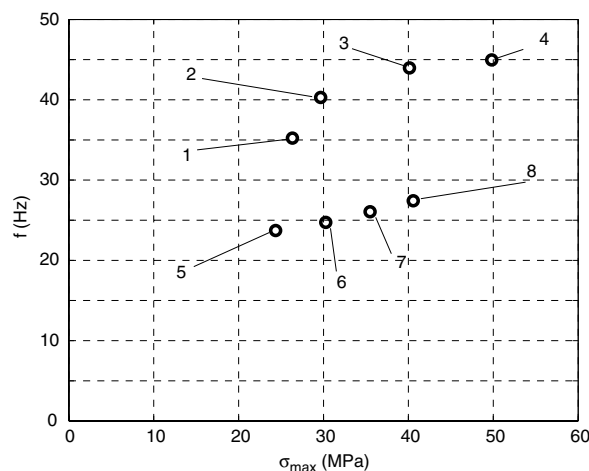


Fig. 6 Trade off between f and σ_{max} for Configuration B.

Consider the optimal configuration with $\sigma_0 = 40$ MPa, i.e. point 3 in Figure 6; this configuration has $w = 40$ mm. Dividing w by 2 results in a 40% decrease in f , see point 8.

Points 5-8 in Figure 6 show clearly that the rate of increase in f in the optimal configurations is much lower than the associated increase in σ_0 ; the slope of a

Table 2 Optimal configurations

Point	α (deg)	β (deg)	γ (deg)	w (mm)	f (Hz)	σ_{max} (MPa)
1	0.1	14.9	93.7	39.5	35.2	26.2
2	2.3	13.2	90.3	40.0	40.2	30.0
3	0.5	9.1	88.9	40.0	43.8	40.1
4	0.5	6.8	88.6	39.8	45.0	49.7
5	6.1	17.4	88.1	20.0	24.0	25.3
6	4.0	14.8	87.9	20.0	24.8	30.5
7	4.1	11.4	87.5	20.0	26.2	35.4
8	2.8	10.6	86.7	20.0	27.0	40.5

Table 3 Mass and frequency for $\sigma_{max} = 25$ MPa

w (mm)	Additional Mass (% of original)	f/f_0 (Hz)
20	16	4.1
30	24	5.3
40	33	5.9

best-fit line through points 5-8 is $\approx 1 : 5$. The gentle slope of this line, compared to the sharp curve between points 1-3, is due to the fact that the configurations with $w = 20$ mm are able to reach the maximum attainable stiffness for the given stress limit, whereas the configurations with $w = 40$ mm are governed by the stress limit.

In conclusion, the general trend is

- if σ_0 is the controlling factor, $\theta \geq 90$ deg;
- if σ_0 is easily achievable, $\theta \leq 90$ deg.

This is because pointing the skirt below the level of the rim of the unstiffened dish is a more efficient way of increasing the stiffness against first-mode deformation, but also produces higher stress levels during folding.

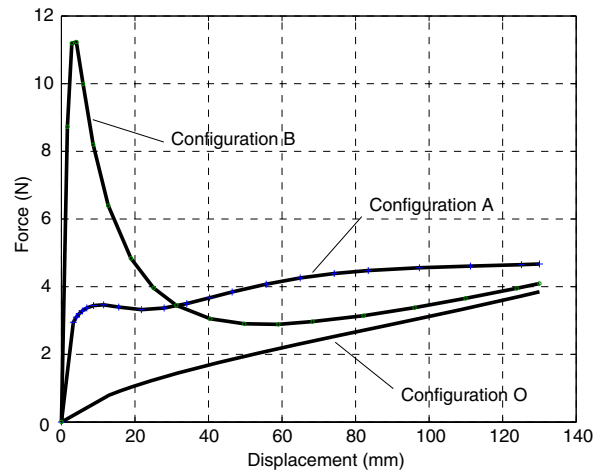
The highest stresses in a folded reflector tend to concentrate around the edge of the slit; about 90% of the structure is typically at a stress that is 40% lower. It should be noted that—in calculating the highest stress—the elements at the tips of the slits have been ignored as there is a stress concentration that could be removed simply by rounding the sharp end of the slits, as shown in Figure 9.

Since PETG has an ultimate failure stress of around 50 MPa, it was decided to choose $\sigma_0 = 25$ MPa. At this point, the final choice of w involved a trade-off between added mass and stiffness increase. Table 3 compares three different configurations, all with a stress limit of 25 MPa.

A similar optimization study was carried out for Configuration A, with two cuts across the skirt and four slits subtending equal angles. This configuration tends to suffer from higher stress concentrations, and so it is more difficult to find design parameters for which the yield stress of the material is not exceeded. To alleviate this problem, the six most highly stressed nodes in the finite element model, which correspond to

a small area around the tip of the cut, were disregarded in the calculation of σ_{max} , again on the grounds that high stress concentration issues could be dealt with by a more careful design of the details. The outcome is that all optimal designs for this configuration have $\gamma > 90$ deg, which as explained earlier has the effect of lowering σ_{max} at the expense of decreasing the bending stiffness in the deployed configuration.

Figure 7 compares the force-displacements relationships of two optimized configurations, A and B, with that of the original configuration, O. Note that the displacement plotted on the abscissa is for only one edge of the dish, hence the distance between the edges that are brought together during folding changes by twice this amount. Both of the optimized configurations have $\sigma_{max} = 49.6$ MPa and $w = 40$ mm. Configuration A has $\alpha = \beta = 0.5$ deg, $\gamma = 95$ deg, and $f = 17.6$ Hz. Configuration B has $\alpha = 0.5$ deg, $\beta = 6.8$ deg, $\gamma = 89$ deg, and $f = 45$ Hz..

**Fig. 7 Comparison of three configurations.**

Note that both configuration A and B are much stiffer than O near the origin, but then snap and for larger displacements tend towards the force-displacement curve of Configuration O. The force required to hold these reflectors fully folded is only a little higher than for the original reflector, by 12% for Configuration A and 7% for Configuration B. It should be noted that the snapping behaviour that is exhibited by these optimized designs is generally not seen in non-optimized structures.

In conclusion, Configuration B has the most promise and makes it comparatively easy to achieve a high stiffness with stresses below any given limit. This is because this configuration allows longer slits in the regions of highest elastic curvature of the reflector, which has the effect of distributing the strain over a wider region thus decreasing the peak strain. On the other hand, the presence of a radial cut in the skirt, in Configuration A, tends to form a hinge-like region along the axis of bending, which is responsible for higher,

Table 4 Tested configurations

Configuration	Cuts	Slits	α (deg)	β (deg)	γ (deg)	w (mm)
O	-	-	-	-	-	-
A	2	2	-	4	50	20
B	-	4	8	24	90	20

localised strains.

Another attractive feature of Configuration B is that the two longer slits leave two long “struts” along the edge of the dish, which buckle and provide the desired snapping behaviour. This has the effect of lowering the peak stresses in the fully-folded structure to a level comparable to that of the original, unstiffened dish.

Experimental Verification

In order to verify selected results from the optimization study, two types of experiments were carried out on small scale physical models:

- static compression tests, to characterize both the initial stiffness of the structure and the force-displacement relationship during folding;
- vibration tests, to measure the natural frequencies of the structure.

The experiments were carried out on PETG dishes made by vacuum forming on parabolic moulds with conical edges. The exact dimensions of these moulds were, diameter $D = 452$ mm, focal length $F = 134$ mm and skirts angles of 50 or 90 deg. Further details are given in Table 4.

The static tests were carried out in an INSTRON testing machine with specially machined fittings; the set up is shown in Figure 8. The connection between the rim of the dish and the INSTRON is through a 2 mm diameter ball and socket joint, which ensures that the edge of the dish is free to rotate through a large angle during folding; a detailed view is shown in Figure 9.

Modal identification tests were carried out by applying a random dynamic excitation to the dishes with a O86D80 ICP impulse hammer fitted with a piezoelectric head, and by measuring the response of the dish at nine points with a Polytec PSV300 scanning laser vibrometer. To reduce noise, each measurement was repeated three times and the results were averaged. After measuring all the target points, the Fast Fourier Transform (FFT) of the above signals was computed in order to obtain the frequency response functions and the mode shapes.

An indication of the accuracy and validity of this type of experiment is provided by the coherence, which is the ratio of the frequency response functions (details in reference^[12]), varying between 1 and 0. A good experiment should normally lead to values close to 1.

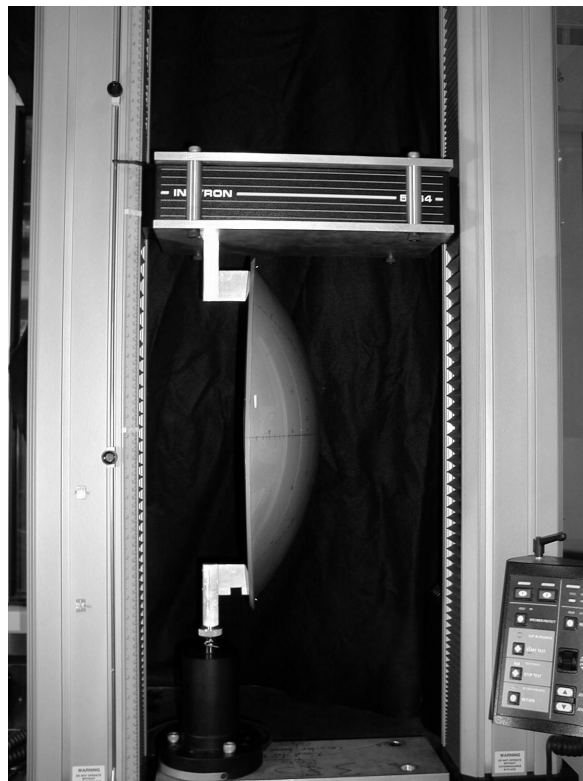


Fig. 8 Static test set up.

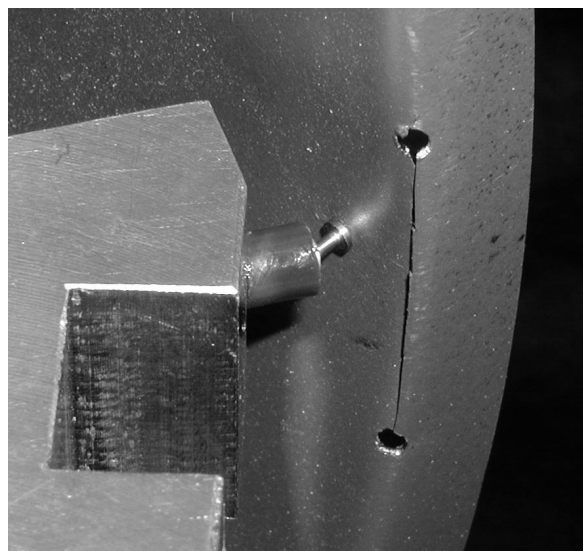


Fig. 9 Detail of dish connection.

This was extremely difficult to obtain for the unstiffened dish, which has an infinite number of symmetric modes; hence for this test only the coherence was neglected. Reasonable values were obtained for tests of the other two configurations, but only after carefully adjusting the boundary conditions.

The mode of greatest interest is the lowest bending mode and hence frequencies for this mode are presented in Table 6, in the section Results and Dis-

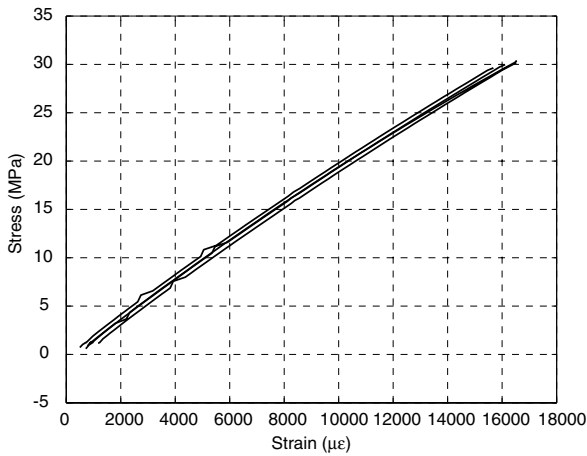


Fig. 10 Stress-strain relationship of PETG.

cussion.

Two different types of boundary conditions were used, as follows. (i) Dish vertical, clamped through the centre to a block; and (ii) dish horizontal and facing up (“cup up”), suspended from three vertical cords. The lengths of the elastic suspension cords were such that the rigid-body vertical mode had a frequency of 1 Hz, to separate the rigid body modes from the flexural modes (which have frequencies of around 10 Hz). Horizontal elastic ties were used to prevent large rigid body motions in the horizontal direction.

Experimental Complications

Early on it had been verified that the behaviour of PETG is very close to linear for stresses in excess of 25 MPa, see Figure 10. The material properties quoted in the Section “Optimization Results” were obtained from specimens cut from the same sheets from which the models had been made.

Several important issues had to be addressed before the finite-element results could be properly validated. They are discussed next.

Geometric Inaccuracies

Although the dishes were all manufactured out of 1 mm sheet, the vacuum-forming process stretches the material and hence the thickness of the model will not be uniform. One would expect the deformation of the material to be axi-symmetric, hence the thickness at the centre of the dish should be 1 mm decreasing radially outwards.

Figure 11 is a graph of the thickness of the dish at the intersection between 28 circumferential lines and 8 radii, measured with a dial gauge. Note that the last two points on each curve are on the skirt. These measurements follow the expected variation from the centre of the dish, but also show a considerable asymmetry; the maximum discrepancy between points on the same circumference is 0.2 mm.

Considering that the flexural stiffness of a shell is proportional to the cube of the thickness, this variation

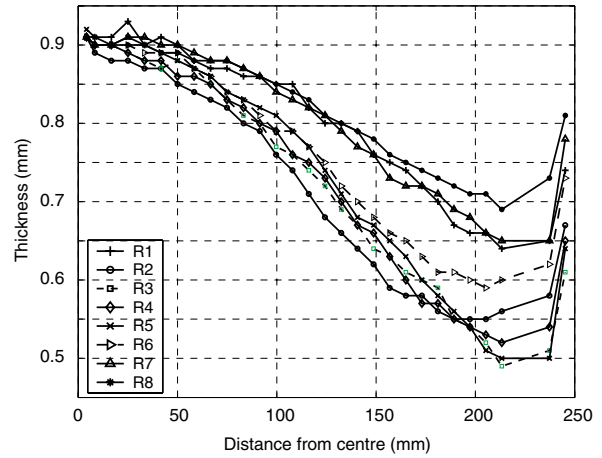


Fig. 11 Thickness of Configuration B dish.

is not negligible. Since it would have been impossible to manufacture dishes with uniform thickness using vacuum forming, the measured thickness distributions had to be incorporated into the computational model. Assuming an axi-symmetric distribution would have been insufficiently accurate, hence the only way of proceeding was to define the thickness of each and every node. Thus, the measured thickness distribution had to be mapped onto the finite element mesh using a specially-written computer program. The thicknesses at the nodes were then included into the ABAQUS model by a “*Nodal Thickness” command.

Mode Shapes and Gravity Effects

Although in the finite element model the dish is clamped at the centre, the rigid-body modes still show very clearly as the first three modes, see Figure 12. These modes are more significantly affected by gravity, see Table 5. However, gravity effects on the bending modes, i.e. modes number 4 and 5, are quite small.

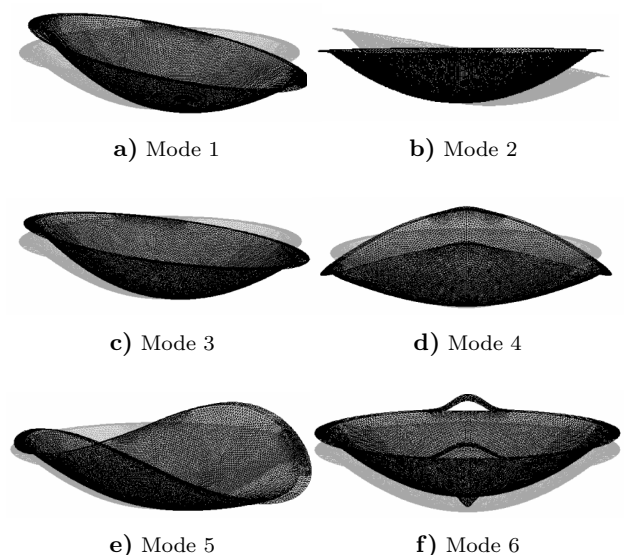


Fig. 12 Mode shapes of centrally clamped Configuration B dish.

Table 5 Effect of gravity on frequencies (Hz) of clamped Configuration B dish

Mode	No gravity	Horizontal (cup up)	Horizontal (cup down)	Vertical
1	2.0	1.7	2.1	1.9
2	2.0	1.7	2.2	2.0
3	2.1	2.1	2.2	2.2
4	16.6	16.8	16.4	16.6
5	18.7	18.8	18.5	18.6
6	41.4	37.3	44.3	38.5

Air-Structure Interaction

When a vibrating structure is immersed in a fluid, it will invoke vibrations in the fluid surrounding it. If the acoustic wavelength is larger than the structural wavelength, a layer of air moves together with the structure; this air thickness decreases as the frequency of vibration increases. This added-mass effect can significantly reduce the lower natural frequencies of a lightweight structure. In order to account for this interaction, one needs to estimate the added mass of air.

Assuming that the first bending mode of a shallow shell can be reasonably approximated with the first bending mode of a flat, circular plate, we can obtain a quick estimate of the natural frequency of interest, ω ^[13]

$$\omega = k^2 t \sqrt{\frac{E}{3\rho(1-\nu^2)}} \tag{6}$$

where k is the wave number, and E, ν, ρ, t are the Young’s Modulus, Poisson’s ratio, density and thickness of the shell, respectively. Solving for k , we get

$$k = \sqrt{\frac{\omega}{t}} \left(\frac{3\rho(1-\nu^2)}{E} \right)^{\frac{1}{4}} \tag{7}$$

A simple estimate of the air thickness that participates in the vibration of the plate is ρ_{air}/k ^[14] and, considering that the plate has air on both sides, we obtain the following expression for the added mass, m_a

$$m_a = \frac{2\rho_{air}}{k} \pi r^2 \tag{8}$$

where r is the radius of the plate.

Finally, assuming that this added mass does not change the shape of the mode of interest, the natural frequency of the structure in air, f_{air} , is given by:

$$f_{air} = f_{vacuum} \sqrt{\frac{m_s}{m_s + m_a}} \tag{9}$$

Here m_s is the total mass of the plate and f_{vacuum} is the frequency of the structure in vacuum, estimated by ABAQUS.

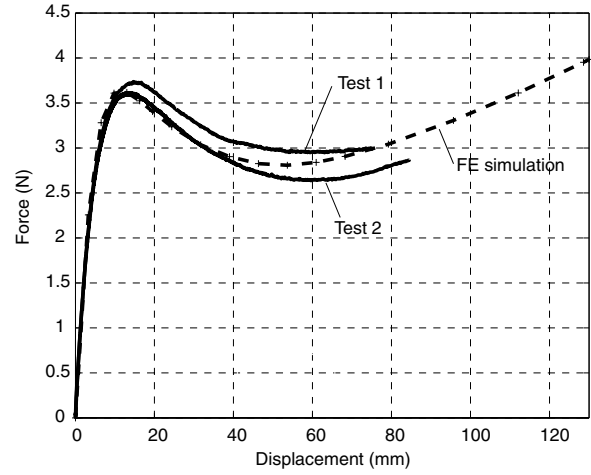


Fig. 13 Comparison of two tests on Configuration A dish with FE analysis.

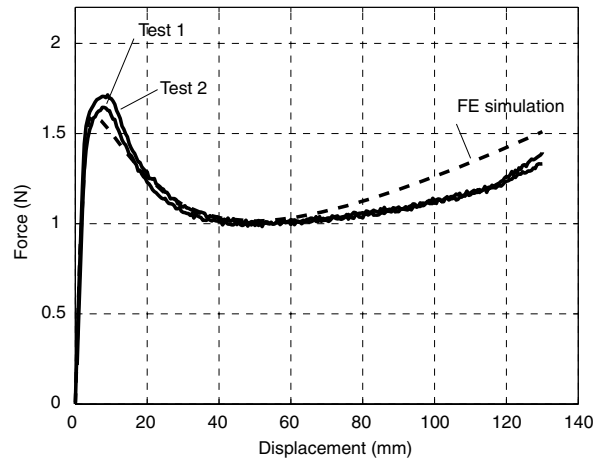


Fig. 14 Comparison of two tests on Configuration B dish with FE analysis.

Results and Discussion

Figures 13 and 14 show the force-displacement plots of the two stiffened configurations that were tested — see Table 4 for details on the corresponding design parameters— and compares them to the ABAQUS simulations. Note that both tests of the Configuration A dish were stopped before attaining the completely packaged shape, to prevent permanent damage of the dish.

In both cases there is excellent correlation between experimental and computational results. The initial slope of the graphs, corresponding to the stiffness of the dishes, has been simulated very accurately.

Note that there is a 4% experimental scatter in the peak force of the Configuration A dish, Figure 13, which tends to increase in the post-buckling range. In Figure 14 the scatter is smaller, and it can be noted that the experimental model buckles marginally later and at a slightly larger load. Considering that we are dealing with the large-displacement behaviour of thin shell structures, which are notoriously challenging

Table 6 Frequency results (Hz)

Configuration	Exp.	ABAQUS (vacuum)	ABAQUS (air)	Error (%)
O	5.0	5.8	4.8	4.4
A	14.9	17.0	15.0	1.1
B	15.4	16.8	14.9	3.3

to model, these discrepancies are too small to worry about.

The following observations, made during the course of the experiments, may provide useful guidance for the detailed design of the stiffening system, in future.

- Defining the position of the origin, i.e. the configuration of zero displacement and zero force was not a trivial issue. This is because the structure had to be held vertically during the tests and self-weight deformation could not be easily cancelled.
- Contact between the buckled skirt and the back of the dish occurs during the final stages of the folding process.
- The long slits in the Configuration B dish, which has $\beta = 24$ deg, leave two long unsupported lengths of skirt. Thus, there are two long and narrow flat strips which never regain in full their original shape. Changing their cross-sectional shape to slightly curved may stabilize them without affecting the folding behaviour of the dish.

Table 6 lists the measured frequencies of the first bending mode of the three configurations listed in Table 4. For Configuration B the measurements were taken with the dish suspended horizontally “cup up”. These values are compared first with the ABAQUS predictions in vacuum and then with the frequencies modified to account for the added mass of air, according to Equation 9. The last column gives the error between the measurements and the predicted frequencies in air.

The results presented in this section have provided an experimental validation for the finite element simulation technique used for the optimization study. Thus, having confirmed that both the large displacement load-displacement relationship and the first bending frequency of a stiffened reflector were computed very accurately by the simulation, it can now be expected that the predictions will be equally accurate for other designs of stiffened reflectors.

Of the two stiffened reflectors that have been tested, neither of which had particularly well optimized design parameters, Configuration B has been confirmed to be the most promising. Although the two configurations have achieved essentially identical stiffness and natural frequency in the deployed configuration, the Configuration A dish gave some concern during folding, and so the fully-folded configuration was never reached for

this one. On the other hand, the Configuration B dish was folded many times without difficulty.

Conclusions

The stiffness in the deployed configuration of a Spring Back Reflector can be increased significantly without compromising its ability to fold elastically.

A particular stiffening system has been proposed and evaluated. In its most successful implementation, it consists of a thin-walled conical shell structure that is attached to the edge of the reflector dish.

By introducing short discontinuities between the dish and the stiffening element, the behaviour of the stiffening system can be tuned in order to maximize the increase in stiffness in the deployed configuration while minimizing the increase in the maximum stress in the fully-folded configuration.

Determining the optimal parameters, i.e. the width and angle of the stiffening structure as well as the length of the discontinuities along the attachment to the dish, requires extensive non-linear finite element simulations and a careful optimization. However, as a first approximation a flat stiffening structure perpendicular to the axis of the reflector is likely to be near-optimal.

Ten-fold increases in stiffness and three-fold increases in the first bending frequency of a small-scale reflector have been verified experimentally. Optimized designs with 80-fold stiffness increases and 8-fold frequency increases have been shown to be possible. Preliminary results for full-scale reflectors, not shown in this paper, suggest that similar improvements can be achieved at full scale.

Acknowledgements

We thank Professor C.R. Calladine and Dr G.T. Parks for helpful suggestions and Dr A. Britto for advice on the computational work. LTT thanks the Cambridge Commonwealth Trust, Emmanuel College, and the Zonta International Foundation for financial support.

References

- ¹Seitz, P., “Spar resolving spat over antenna work,” *Space News*, Aug. 29-Sept. 4 1994.
- ²Anonymous, “Hughes graphite antennas installed on MSAT-2 craft,” *Space News*, November 1994.
- ³Greschik, G., “On the practicality of a family of pop-up reflectors,” *9th Annual AIAA/Utah State University Conference on Small Satellites*, 18-21 September 1995.
- ⁴Hooke, R. and Jeeves, T.A., “Direct search solution of numerical and statistical problems,” *Journal of ACM*, Vol. 8, April 1961, pp. 212–229.
- ⁵Johnson, M.G., “hooke.c,” http://netlib.bell-labs.com/magic/netlib_find?db=0&pat=hooke+jeeves+, C programme.
- ⁶Kaupe, Jr, A.F., “Algorithm 178 direct search,” *Communications of the ACM*, Vol. 6, No. 6, June 1963, pp. 313–314.

⁷Bell, M. and Pike, M.C., “Remark on algorithm 178 [E4] direct search,” *Communications of the ACM*, Vol. 9, No. 9, September 1966, pp. 684–685.

⁸Smith, L.B., “Remark on algorithm 178 [E4] direct search,” *Communications of the ACM*, Vol. 12, No. 11, November 1969, pp. 637–638.

⁹Haftka, R.T. and Gürdal, Z., *Elements of Structural Optimization*, chap. 1, Kluwer Academic Publishers, 1993, pp. 7–9.

¹⁰*ABAQUS Version 6.1*, Hibbitt, Karlsson & Sorenson, 1080 Main Street, Pawtucket, RI 02860-4847, USA, 1998.

¹¹*MSC/PATRAN Version 8.5*, MacNeal-Schwendler Corporation, Los Angeles, California, USA, 1999.

¹²Ewins, D.J., *Modal Testing: Theory and Practice*, John Wiley & Sons Inc., 1995.

¹³Achenbach, J.D., *Wave Propagation in Elastic Solids*, North-Holland Publishing Company, 1976.

¹⁴Kukathasan, S., and Pellegrino, S. “Vibration of Prestressed Membrane Structures in Air,” *43rd AIAA SDM Conference*, Denver, CO, AIAA-2002-1368.